








Incoherent electronic band states in Mn-substituted BaFe₂As₂Marli R. Cantarino ^{1,2,*}, Kevin R. Pakuszewski ³, Björn Salzmänn, ⁴ Pedro H. A. Moya ¹, Wagner R. da Silva Neto ¹, Gabriel S. Freitas, ³ P. G. Pagliuso, ^{3,5} Walber H. Brito ⁶, Claude Monney ⁴, C. Adriano, ³ and Fernando A. Garcia ^{1,†}¹*Instituto de Física, Universidade de São Paulo, 05508-090 São Paulo, SP, Brazil*²*Brazilian Synchrotron Light Laboratory (LNLS),**Brazilian Center for Research in Energy and Materials (CNPEM), Campinas-SP, 13083-970, Brazil*³*Instituto de Física “Gleb Wataghin”, UNICAMP, 13083-859, Campinas-SP, Brazil*⁴*Département de Physique and Fribourg Center for Nanomaterials, Université de Fribourg, CH-1700 Fribourg, Switzerland*⁵*Los Alamos National Laboratory, Los Alamos, New Mexico 87545, USA*⁶*Departamento de Física, Universidade Federal de Minas Gerais, C.P. 702, 30123-970, Belo Horizonte, MG, Brazil*

(Received 6 March 2023; revised 3 October 2023; accepted 16 November 2023; published 8 December 2023)

Chemical substitution is commonly used to explore new ground states in materials, yet the role of disorder is often overlooked. In Mn-substituted BaFe₂As₂ (MnBFA), superconductivity (SC) is absent, despite being observed for nominal hole-doped phases. Instead, a glassy magnetic phase emerges, associated with the $S = 5/2$ Mn local spins. In this work, we present a comprehensive investigation of the electronic structure of MnBFA using angle-resolved photoemission spectroscopy (ARPES). We find that Mn causes a small and orbital-specific reduction of the electron pockets, only partially disrupting nesting conditions. Based upon the analysis of the spectral properties, we observe, for all bands, an increase in the electronic scattering rate as a function of Mn content. This is interpreted as increasing band incoherence, which we propose as the primary contributor to the suppression of the magnetic order in MnBFA. This finding connects the MnBFA electronic band structure properties to the glassy magnetic behavior observed in these materials and suggests that SC is absent because of the collective magnetic impurity behavior that scatters the Fe-derived excitations. Additionally, our analysis shows that the binding energy (E_B) dependence of the imaginary part of the self-energy [$\text{Im}\Sigma(E_B)$] is best described by a fractional scaling ($\text{Im}\Sigma(E_B) \propto \sqrt{-E_B}$). These results indicate that Mn tunes MnBFA into an electronic disordered phase between the correlated Hund’s metal in BaFe₂As₂ and the Hund’s insulator in BaMn₂As₂.

DOI: [10.1103/PhysRevB.108.245124](https://doi.org/10.1103/PhysRevB.108.245124)**I. INTRODUCTION**

Electronic correlated materials exhibit a rich phase diagram when subjected to partial chemical substitution of one of their constituting elements. Whereas a great deal of attention is devoted to superconducting (SC) phases driven by this strategy, non-SC phases also spark heated debate. One such example are the Ba(Fe_{1-x}Mn_x)₂As₂ materials which derive from the parent compound BaFe₂As₂ (BFA).

BFA is an Iron-based superconductor (IBS) material [1]. This system undergoes nearly simultaneous phase transitions from a tetragonal to an orthorhombic phase, and from a paramagnetic (PM) to a spin density wave (SDW) phase with a critical temperature (T_{SDW}) of about 134 K [2]. A high-temperature SC phase can be driven in BFA by multiple partial chemical substitution strategies [1,3–8], including nominal hole doping [9,10], which invites an explanation for the absence of SC in Mn substituted BFA (MnBFA) [11–13].

Whereas it was proposed that SC is absent in MnBFA because the Mn-derived states remain localized and therefore charge doping is not caused by Mn substitution [14,15], the scattering of the Fe-derived SDW fluctuations by the Mn-derived Néel fluctuations is also believed to play the key role [16,17] in this phenomenology. The latter topic further invites an investigation into the relative relevance attributed to disorder or magnetic and impurity scattering [18–20] caused by Mn.

Despite the absence of charge doping, changing electronic bands in MnBFA cannot be discarded since the hybridization between Fe and As states depends on Mn content [21]. Indeed, the electronic structure cannot be totally independent of the Mn content, since MnBFA is tuned to a Hund’s insulating state in BaMn₂As₂ [22–24]. Our motivation is thus to fill an important gap in this discussion: the detailed characterization of the electronic band structure of MnBFA samples, which is so far lacking despite previous experimental efforts [15]. Employing an alternative In-flux method [25], we grew high-quality MnBFA single crystals and performed angle-resolved photoemission spectroscopy (ARPES) experiments of Ba(Fe_{1-x}Mn_x)₂As₂ ($x = 0.0, 0.035$ and 0.085 , hereafter called BFA, Mn3.5% and Mn8.5% samples, respectively). We find that Mn causes a sizable decrease in the electron pockets,

*Present affiliation: European Synchrotron Radiation Facility, BP 220, F-38043 Grenoble Cedex, France; Corresponding author: marli.cantarino@esrf.fr

†Corresponding author: fgarcia@if.usp.br

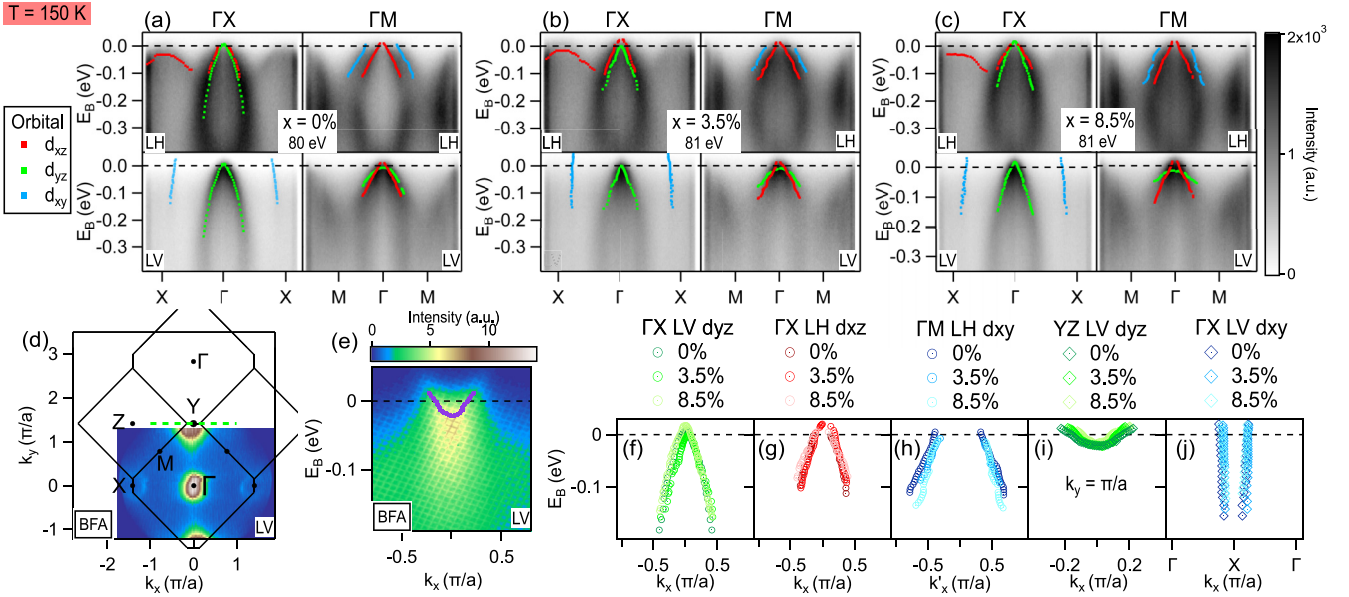


FIG. 1. (a)–(c) Overview of the measured electronic band maps of the BFA, Mn3.5%, and Mn8.5% materials at $T = 150$ K. Measurements were taken along the ΓX and ΓM directions and for LH and LV polarizations, as indicated. The dots represent points fitted to the second derivative (see [29]). (d) BFA Fermi surface measured with LV polarization with the BZ drawn and its high-symmetry points indicated. The green dashed line indicates the cut based upon which the electron pocket of (e) was reconstructed. (f)–(j) Bands obtained from MDC fits for different Mn content focusing on states close to E_F . The experimental conditions are indicated for each panel.

which partially tunes the system out of the nesting condition and contributes to the suppression of T_{SDW} . The absence of charge doping in MnBFA is thus put into question.

Our results derived from the analysis of the spectral properties, however, suggest that the suppression of T_{SDW} is mainly an effect of disorder and magnetic scattering, both of which combine to preclude the formation of a SC ground state [18–20]. Our findings support that the indirect exchange interaction between the Mn local moments is mediated by incoherent electronic states, explaining the glassy behavior of the Mn local moments [26]. Moreover, we find that the imaginary part of the self-energy [$\text{Im}\Sigma(E)$] displays a fractional scaling as a function of the binding energy (E_B), characterizing the MnBFA as a Hund’s metal [27,28].

II. MATERIALS AND METHODS

$\text{Ba}(\text{Fe}_{1-x}\text{Mn}_x)_2\text{As}_2$ single crystals were grown using the In-flux method [25]. All samples were characterized by resistivity, powder x-ray diffraction (XRD), and energy-dispersive x-ray spectroscopy (EDS) to obtain T_{SDW} , lattice parameters, and chemical composition, respectively. The final Mn content (x) was characterized by energy-dispersive x-ray spectroscopy (EDS) and by comparing the sample’s T_{SDW} to other x vs T phase diagrams in literature [12,14] to benchmark the EDS determined values of x .

The ARPES experiments were performed at the Bloch beamline of the Max IV synchrotron in Lund, Sweden, using the Scienta DA30 photoelectron analyzer. The total energy resolution was set at about 8 to 10 meV for incident photon energies between 60 and 81 eV, and angular resolution of 0.1° . The samples were cleaved using Al posts inside the main preparation chamber (vacuum of 3×10^{-10} mbar) and then

transferred to the analyzer chamber (vacuum of 2×10^{-11} mbar) for the experiments. For all samples, measurements were performed at 150 K and 20 K, corresponding to above and below T_{SDW} , respectively. The cooling was performed through a six-axis cryo manipulator using a closed-cycle liquid Helium system.

Our ARPES experiments were carried out along the high symmetry directions ΓX and ΓM for both Γ and Z k_z levels. The high symmetry points are labeled with respect to the body-centered tetragonal crystal structure. Linear horizontal (LH or π) and vertical (LV or σ) polarized x-rays were used to probe different Fe-3d orbital contributions to the ARPES signal. The final polarization state, and its respective ARPES selection rule, depend on the parity of the product between each orbital and the x-ray polarization with respect to the photoemission mirror plane [30–33].

III. RESULTS AND DISCUSSION

A. Paramagnetic state results

In Figs. 1(a)–1(c), we present a survey of the electronic band structures, as a function of Mn content, in the tetragonal PM state ($T = 150$ K) of our samples. Measurements were taken along the high-symmetry directions and adopting linear beam polarizations, either linear horizontal (LH) or linear vertical (LV), as indicated in each panel. The crystal body-centered tetragonal geometry was adopted to label the Brillouin zone (BZ) high-symmetry points.

Band features are distinguishable for all samples, allowing a comprehensive characterization of the MnBFA electronic bands. In the simplest model, the IBS electronic bands derive from Fe 3d states that are subjected to the effects of the As

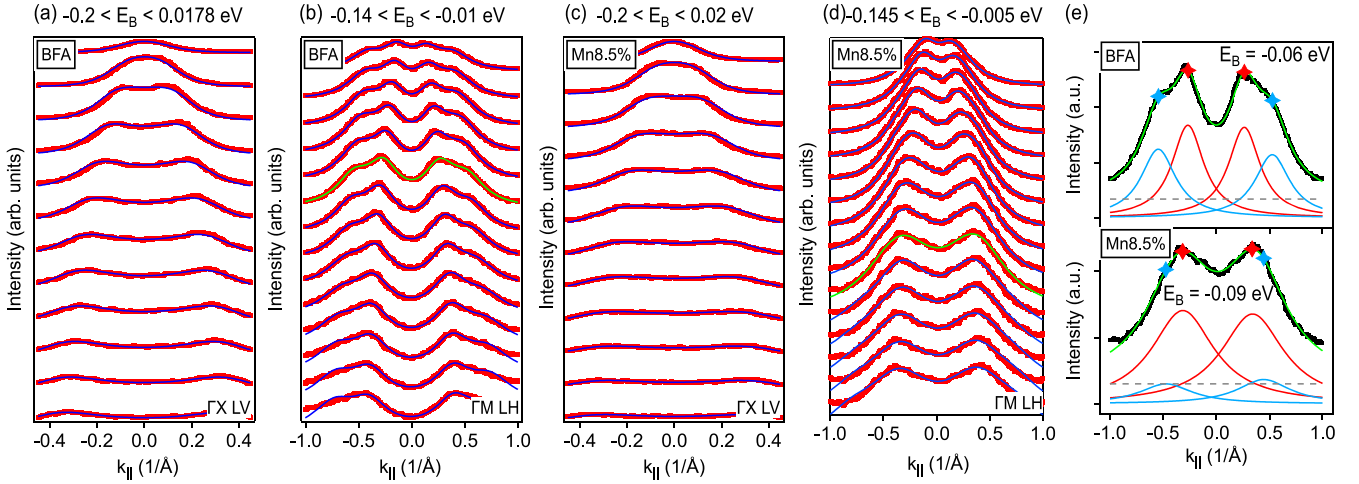


FIG. 2. ARPES spectral function analysis. Fittings (blue lines) of several MDCs (red dots) for increasing binding energies. Data obtained for BFA adopting (a) LV polarization, measured along ΓX and (b) LH polarization, measured along ΓM . In panels (c) and (d) the respective fittings for the Mn8.5% sample are presented. In panels (b) and (d) the MDCs are due to two bands and therefore four Lorentzian peaks are included in the fittings. Details of this procedure for the representative MDC spectra highlighted in green in (b) and (d) are presented, respectively, in the upper (BFA) and lower (Mn8.5%) panels of (e).

ligands, which break the Fe $3d$ states degeneracy and instill a strong orbital character to the electronic bands [1,34]. Based upon the selection rules for the ARPES intensity polarization dependence and guided by previous works [30–33,35,36], the orbital character of the electronic bands were labeled.

The effects of Mn substitution on the electronic bands are examined in Figs. 1(f)–1(j). We focus on states close to E_F . To characterize how the hole pockets change as a function of Mn content, we track the hole bands with main $d_{xz/yz}$ and d_{xy} orbital character close to Γ and measured along the high-symmetry directions [Figs. 1(a)–1(c)]. Results are presented in Figs. 1(f)–1(h). Electronic states at the electron pockets around the X/Y points, however, have C_{2v} point symmetry which is reflected in the idealized elliptical shape of the pockets. Therefore, we must also look at the bands in a direction perpendicular to the ΓX direction. We consider a cut in our Fermi maps along the green dashed line shown in Fig. 1(d), for the BFA case, representing the YZ direction. The associated electronlike band is shown in Fig. 1(e) and is called the “shallow” electronlike band as opposed to the “deep” electronlike band observed directly in Figs. 1(a)–1(c), as the blue points for ΓX and LV polarization. The shallow (deep) electronlike band determines the minor (major) semiaxis of the electron pocket around X/Y and has d_{yz} (d_{xy}) main orbital character. In Figs. 1(i) and 1(j) we compile the deep and shallow electronlike bands as a function of Mn content.

In the rigid band shift picture, increasing hole pockets and shrinking electron pockets are the putative effects of hole doping caused by Mn. By inspection of Figs. 1(f)–1(j), the experimentally determined scenario is more involved. Bands forming the hole pockets and the deep electronlike band are barely affected [Figs. 1(f)–1(h)], whereas the intersection of the shallow electronlike band (d_{yz} orbital character) with E_F (which determines k_F) is systematically decreasing. Our experiments thus reveal that Mn can contribute holes to BFA but not in a way that can be described as a rigid band shift. We suggest that it is the effect of the changing

Fe $3d_{yz/xz}$ and As $4p_z$ hybridization as a function of Mn content [21,22].

Assuming the scenario wherein the SDW phase is stabilized by the nesting between hole and electron states [34,37], the Mn8.5% effect on the shallow electronlike band is comparable, albeit in the opposite direction, to that caused on the electron pockets by nearly the same amount of Co ($x_{Co} = 0.08$) [38]. For $x_{Co} = 0.08$, however, the SDW is already absent, because Co also causes the hole pockets to shrink, tuning CoBFA off the nesting condition. If one chooses a comparison between systems with the same T_{SDW} , our Mn8.5% sample ($T_{SDW} = 66$ K) is closer to $x_{Co} = 0.045$ ($T_{SDW} = 65$ K). Again, one finds [38] that the main source of a partial detuning of the nesting condition is the simultaneous change in electron and hole pockets. Therefore, whereas the electronic tuning caused by Mn may contribute to the suppression of the SDW phase, it cannot be the dominant effect.

We thus resort to a quantitative analysis of the ARPES spectral function to probe for other effects of the Mn substitution. We fit momentum distribution curves (MDCs) to the expression for the one-particle spectral function $A(\mathbf{k}, E_B)$ for a system of weakly correlated electrons [39]. Our objective is to extract the electronic scattering rate $\Gamma(E_B)$ and the imaginary part of the self-energy $\text{Im}\Sigma(E_B)$, both as a function of the binding energy E_B . We concentrate on extracting $\Gamma(E_B)$ and $\text{Im}\Sigma(E_B)$ from the MDCs analysis for the bands with d_{yz} and d_{xy} main orbital character in the measurements in direction ΓX with LV polarization and ΓM with LH polarization, respectively, represented as green and blue hole pockets of Figs. 1(a)–1(c).

The fittings are presented in Figs. 2(a)–2(d) for the BFA and Mn8.5% samples. The fittings in Figs. 2(a) and 2(c) (band of d_{yz} orbital character) were obtained as in Refs. [40,41], whereas the fittings in Figs. 2(b) and 2(d) were obtained as explained in the Supplemental Material [29] (see also Refs. [42–52] therein). The later spectral features are due to two bands of d_{xy} and d_{xz} orbital

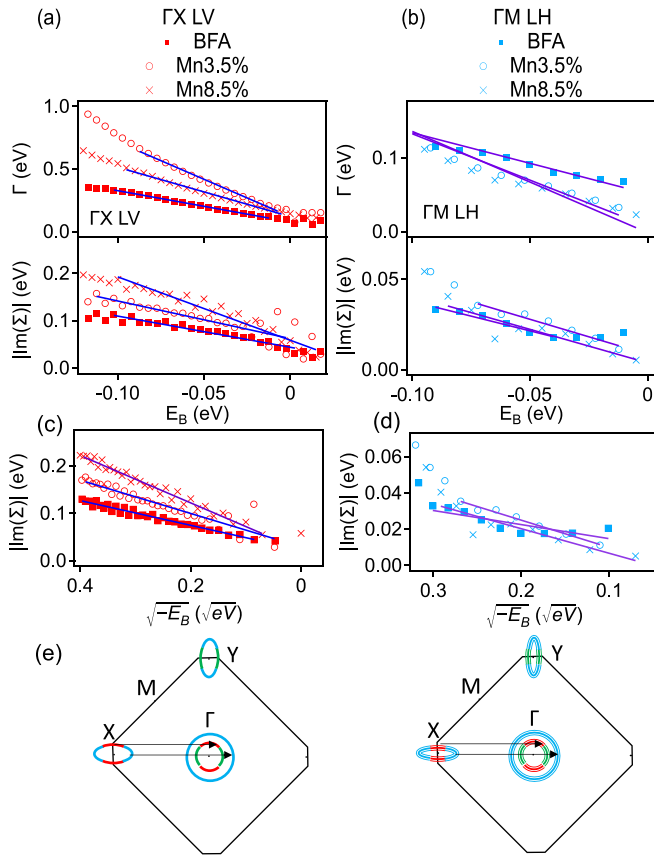


FIG. 3. The extracted quantities $\Gamma(E_B)$ and $\text{Im}\Sigma(E_B)$ for all three samples obtained for (a) LV polarization, measured along ΓX and (b) LH polarization, measured along ΓM . (c)-(d) Respectively, the $\text{Im}\Sigma(E_B)$ data presented in (a) and (b) but plotted as a function of $\sqrt{-E_B}$. (e) Schematic summary of the experimentally determined effect of Mn on MnBFA electronic band structure.

character (see Fig. 1), and require the use of four Lorentzian lineshapes. In Fig. 2(e), fitting details for two representative cases, BFA and the Mn8.5% samples, are shown. The need of four lineshapes is clear in both cases, although the spectral features are better defined in the BFA case because of the smaller lineshape broadening. Reliable fittings of the doped samples' spectra were achieved by adopting the results presented in Fig. 1 as inputs to find the center of the distributions in our spectral analysis.

The extracted values of $\Gamma(E_B)$ and the calculated $\text{Im}\Sigma(E_B)$ are shown, as a function of E_B , in Figs. 3(a) and 3(b) for all samples. The broadening of the spectroscopic features, here measured by $\Gamma(E_B)$, contains intrinsic and extrinsic effects which also affect the determination of $\text{Im}\Sigma(E_B)$. A way around this problem is to focus on the rate of change and scaling properties of these quantities, which are less affected by the homogeneous broadening introduced by extrinsic effects. This is qualitatively captured by the lines drawn in Figs. 3(a) and 3(b), which serve as guides to eyes and suggest that $\Gamma(E_B)$ can be described as a linear function of E_B close to E_F .

Observing the lines, we can see that the rate of change of $\Gamma(E_B)$ increases as a function of Mn content in the cases of both d_{yz} and d_{xy} bands. Certainly, the effect is more prominent

for the d_{yz} band. Physically, $\Gamma(E_B)$ being proportional to the inverse of the quasiparticle lifetime, it is a measurement of the electronic states' coherence. An increasing rate of change thus translates into less coherent electronic band states and this is precisely the observed effect caused by Mn substitution in all bands.

Turning our attention to the lower panel of the same figure, we can see that $\text{Im}\Sigma(E_B)$ only follows a linear scaling very close to E_F . A linear scaling is reminiscent of a marginal Fermi liquid [39,53], and an analysis based upon this picture is carried out in [29] and serves as a source for comparison with previous similar analysis [40,41,54].

Here, we focus on the scaling properties of $\text{Im}\Sigma(E_B)$ in a broader energy interval. As presented in Figs. 3(c) and 3(d), for the energy interval $0.4 > \sqrt{-E_B} > 0$ and $0.3 > \sqrt{-E_B} > 0$, for the d_{yz} and d_{xy} bands, respectively, $\text{Im}\Sigma(E_B)$ presents a fractional scaling as a function of E_B . In the particular case of the d_{yz} bands, an excellent $\text{Im}\Sigma(E_B) \propto \sqrt{-E_B}$ scaling is observed. This type of behavior is the hallmark of a Hund's metal for temperatures above the onset of spin screening, wherein the charge degrees of freedom are itinerant but the spin degrees of freedom retain a local character [22,24,27,28,55]. In our work, this regime is observed in the presence of increasing electronic disorder caused by the Mn substitution.

Thus, the effects caused by Mn substitution amount to (i) a small and orbital-specific shrinking of the electron pockets and (ii) the increase of the electronic bands' incoherence in all bands crossing E_F . The orbital-specific doping effect stems from the interaction between the metal and the ligand orbitals and cannot be put in terms of a rigid band shift or, equivalently, the depleting of the Fe local electronic occupation. Thus, it favors the interpretation that Mn tunes MnBFA from a Hund's metal in BFA to a Hund's insulating state in BaMn_2As_2 [22,24,28] over the Mott scenario, since the latter explicitly proposes a change in the Fe electronic occupation as a way to get into the correlated phase and eventually into a Mott regime in half filling [56–58]. The weak hole doping effect, however, cannot explain the T_{SDW} suppression.

In keeping with the nesting scenario, the emergence of incoherent carriers may act as a mechanism for the T_{SDW} suppression, since the broadening of the electronic states implies incoherent carriers that do not contribute to the nesting condition [59]. Our scaling results, however, characterize MnBFA as a Hund's metal where spins retain a local character. This tendency for localization of the magnetism in MnBFA is captured by optical spectroscopy measurements [60] and, from a phenomenological standpoint, could be related to the almost linear decrease of T_{SDW} as a function of Mn content. In any case, it is suggested that disorder is the main mechanism for the suppression of T_{SDW} , not electronic tuning. It is intriguing that Mn, being close to Fe, behaves similarly to Zn which, in principle, is a much stronger impurity scatter, and not similar to Co [61,62].

The left and right panels in Fig. 2(e) summarize our findings concerning the electronic structure of the PM state. The upper panel shows schematics of the BFA PM Fermi surface. Nested electron and hole states are connected by a (π, π) vector drawn to scale. The lower panel shows the respective

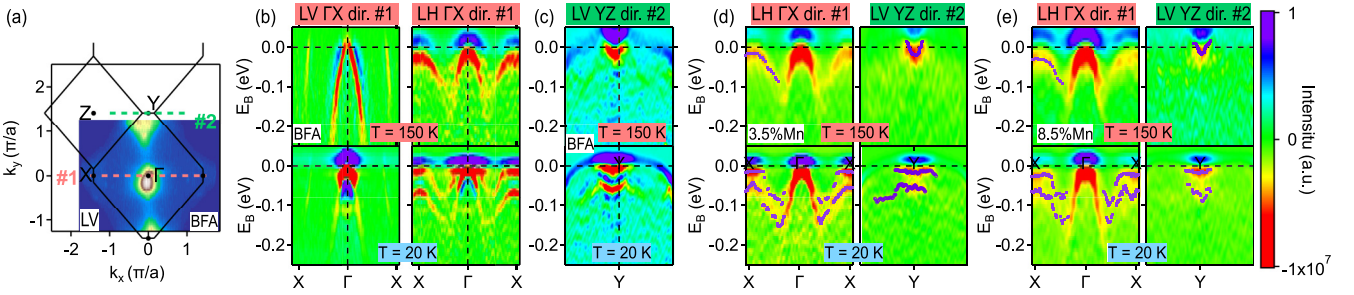


FIG. 4. Second derivatives of high and low-temperature bands of MnBFA sample for different polarization: (a) FS maps showing the cuts, traced in pink and green, for which the bands are shown in panels (b)–(e). (b) ΓX direction and (c) YZ direction second derivatives for the BFA sample. The respective (d) Mn3.5% and (e) Mn8.5% sample results. The directions and light polarization are indicated in each panel and the fitted band points are marked as purple points.

schematics for MnBFA. Mn causes a significant broadening of all electronic states and the shrinking and deformation of the electron pockets, resulting in the partial detuning of the nesting condition.

B. Magnetically ordered state results

We now turn to the reconstructed electronic structures, characterized at $T = 20$ K, well below the magnetic transition. First, we discuss the nematic splitting Δ , between bands with d_{xz} and d_{yz} orbital character, as a function of Mn. In Fig. 4(a), a FS map for the BFA sample (obtained with LV polarization and along ΓX) is shown, wherein cuts along the YZ and ΓX are indicated, respectively, by the green and pink dashed lines. The second derivative of the electronic band maps along these directions are shown in Figs. 4(b) and 4(c) for BFA and Figs. 4(d) and 4(e) for the Mn substituted samples. We could not resolve the reconstructed “petallike” fourfold symmetric shape recently reported [63]. From the YZ cut, we can access Δ of the shallow electronlike band, reported as $\Delta = 40$ meV for the BFA [32]. This splitting, the consequence of breaking the degeneracy of the d_{xz}/d_{yz} electron bands, manifests as well in the almost flat electron band close to the X point, as shown in the lower panel of Fig 4(b). Indeed the entire band appears duplicated along the ΓX direction. Using EDCs to fit the band positions, we superimpose the bands performing a rigid energy shift on the lower duplicated band to estimate Δ , and Fig. 5(a) presents Δ as a function of Mn.

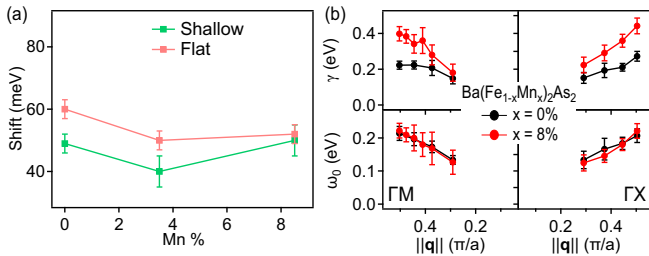


FIG. 5. (a) Nematic splitting size for shallow and flat bands as a function of Mn %. (b) RIXS derived magnon damping coefficients (γ) and bare frequencies (ω_0) for 0% and 8%Mn samples as a function of momentum for two directions.

There is still debate about the nematic splitting size for these materials [64], reported as 60 meV for FeSe thin film [65] and 70 meV for BFA [66], which is in good agreement with our findings. We can observe that for both bands there is no scaling between Δ and T_{SDW} : indeed, Δ decreases only about 20% from its value for BFA whereas T_{SDW} decreases by about 60%. This splitting is currently understood as evidence of nematic ordering and a consequence of the orthorhombic distortion. It is only for $x > 0.1$ that Mn substitution suppresses the orthorhombic transition [12,26,67]. For $x < 0.1$, T_{SDW} and the orthorhombic distortion are intertwined, but the weak Δ dependence on Mn content for $x < 0.1$ does not reflect this phenomenology.

The presented ARPES results can be applied to an in-depth reexamination of previous Resonant Inelastic X-ray Scattering (RIXS) experiments of MnBFA samples [17], which characterized the magnon dispersions along ΓX and ΓM as a function of Mn. In Fig. 5(b), we show the RIXS measured ($T = 20$ K) magnon damping coefficients (γ) and the magnon bare frequencies (ω_0) for BFA and Mn8.0% samples, as a function of the in-plane momentum, $||\mathbf{q}||$, along the main symmetry directions of the 1Fe Brillouin zone. As a function of Mn, ω_0 remains unaffected, whereas γ increases, with the excitations becoming overdamped ($\omega_0 \lesssim \gamma/2$) for almost all values of $||\mathbf{q}||$ in the case of the Mn8.0% sample. This abnormally large magnon damping is not observed in RIXS results for other IBS materials [68–70].

The RIXS measured magnons are due to spin flips associated with the d_{xy} orbitals [71]. Our ARPES data show explicitly that the reconstructed electronic structure is related to an energy scale of the order of 60 meV in the case of BFA. However, the relative change with Mn substitution in Δ is at most 20% of this value, ≈ 12 meV, which is beyond the highest resolution RIXS experiments to date. In this sense, the positioning of the d_{xy} -derived bands in the reconstructed electron structure is also not affected by Mn content, which is compatible with the RIXS measured ω_0 values being not affected by Mn. The magnon damping γ , however, is strongly increased by Mn, suggesting that the cooperative behavior between the Mn local moments and conduction electrons plays the key role in promoting the scattering of the Fe-derived excitations by the short-range Néel fluctuations [17–19]. Therefore, the present observation by ARPES of increasing band incoherence naturally connects with the RIXS results.

IV. CONCLUSIONS AND OUTLOOK

Our experiments and analysis show that Mn causes a sizable hole doping effect, which manifests in the shrinking of electron pockets. The dominant effect of Mn, however, is the increase of electronic incoherence, observed for all bands, as deduced from the behavior of $\Gamma(E_B)$ in the spectral analysis. We suggest that the latter and magnetic scattering [17–19] are the control parameters for the evolution of T_{SDW} . We also show explicitly that Mn causes a sizable effect on the nematic splitting Δ , which decreases with increasing Mn content.

Our findings support that the indirect exchange between Mn local moments is mediated by incoherent electronic states, explaining the glassy behavior of Mn spins [26]. Indeed, as previously observed [12], the suppression of T_{SDW} as a function of Cr and Mn content in substituted BFA does not depend on the nature of the dopant, but the spin glass state of the Mn spins distinguishes the physics of Cr and Mn substitutions. The electronic band incoherence here observed should be a feature only of MnBFA. We should also comment on a recent analysis of Mn and Cr substituted 1144 IBS materials [72,73], which also proposes that the amount of doped holes is not controlling the suppression of T_C and T_{SDW} for these substitutions.

A robust finding of our spectral analysis is the $\text{Im}\Sigma(E_B) \propto \sqrt{-E_B}$ scaling. Whereas this was already observed in the case of the IBS materials [55], our paper highlights the coexistence of this correlated Hund's metal phase with the electronic disorder. In this regard, whereas our findings provide the mechanism for the glassy behavior of Mn spins, the specific proposition of a Griffiths-like phase in MnBFA [26] (or even in Mn substituted SrFe_2As_2 [74]) should be reexamined, since in general grounds it demands proximity to a Mott phase [75–77]. Indeed, the effects of disorder in a Hund's metal re-

mains to be explored and we hope that our work may stimulate this discussion.

Finally, given the entirety of our results, the picture advanced in Refs. [19,20] provide the most complete scenario to explain the absence of SC in MnBFA samples since our work shows that disorder is an integral property of the electronic states in MnBFA.

ACKNOWLEDGMENTS

We thank Eric C. Andrade for fruitful discussions. We acknowledge the MAX IV Laboratory for time on Bloch Beamline under Proposal No. 20200293 and the support of Gerardina Carbone and Craig Polley. Research conducted at MAX IV, a Swedish national user facility, is supported by the Swedish Research council under Contract No. 2018-07152, the Swedish Governmental Agency for Innovation Systems under Contract No. 2018-04969, and Svenska Forskningsradet Formas under Contract No. 2019-02496. The Fundação de Amparo à Pesquisa do Estado de São Paulo financial support is acknowledged by M.R.C. (Grants No. 2019/05150-7 and No. 2020/13701-0); F.A.G. (Grant No. 2019/25665-1); C.M. and B.S. acknowledge funding from the Swiss National Science Foundation (SNSF) Grant No. P00P2_170597. K.R.P., P.G.P., and C.A. (Grant No. 2017/10581-1). P.G.P. and C.A. acknowledge financial support from CNPq: Grants No. 304496/2017-0, No. 310373/2019-0, and No. 311783/2021-0. W.H.B. acknowledges financial support from CNPq: Grant No. 402919/2021-1 and FAPEMIG. Work at Los Alamos was supported by the U.S. Department of Energy, Office of Basic Energy Sciences, Division of Materials Science and Engineering: project “Quantum Fluctuations in Narrow-Band Systems.”

-
- [1] H. Hosono and K. Kuroki, Iron-based superconductors: Current status of materials and pairing mechanism, *Physica C: Superconductivity and its Applications* **514**, 399 (2015), Superconducting materials: Conventional, unconventional and undetermined.
- [2] M. Rotter, M. Tegel, D. Johrendt, I. Schellenberg, W. Hermes, and R. Pöttgen, Spin-density-wave anomaly at 140 K in the ternary iron arsenide BaFe_2As_2 , *Phys. Rev. B* **78**, 020503(R) (2008).
- [3] P. C. Canfield and S. L. Bud'ko, FeAs-based superconductivity: A case study of the effects of transition metal doping on BaFe_2As_2 , *Annu. Rev. Condens. Matter Phys.* **1**, 27 (2010).
- [4] S. Jiang, H. Xing, G. Xuan, C. Wang, Z. Ren, C. Feng, J. Dai, Z. Xu, and G. Cao, Superconductivity up to 30 K in the vicinity of the quantum critical point in $\text{BaFe}_2(\text{As}_{1-x}\text{P}_x)_2$, *J. Phys.: Condens. Matter* **21**, 382203 (2009).
- [5] A. S. Sefat, R. Jin, M. A. McGuire, B. C. Sales, D. J. Singh, and D. Mandrus, Superconductivity at 22 K in co-doped BaFe_2As_2 crystals, *Phys. Rev. Lett.* **101**, 117004 (2008).
- [6] N. Ni, A. Thaler, A. Kracher, J. Q. Yan, S. L. Bud'ko, and P. C. Canfield, Phase diagrams of $\text{Ba}(\text{Fe}_{1-x}\text{M}_x)_2\text{As}_2$ single crystals ($M = \text{Rh}$ and Pd), *Phys. Rev. B* **80**, 024511 (2009).
- [7] S. R. Saha, T. Drye, K. Kirshenbaum, N. P. Butch, P. Y. Zavalij, and J. Paglione, Superconductivity at 23 K in Pt doped BaFe_2As_2 single crystals, *J. Phys.: Condens. Matter* **22**, 072204 (2010).
- [8] L. J. Li, Y. K. Luo, Q. B. Wang, H. Chen, Z. Ren, Q. Tao, Y. K. Li, X. Lin, M. He, Z. W. Zhu, G. H. Cao, and Z. A. Xu, Superconductivity induced by Ni doping in BaFe_2As_2 single crystals, *New J. Phys.* **11**, 025008 (2009).
- [9] M. Rotter, M. Tegel, and D. Johrendt, Superconductivity at 38 K in the iron arsenide $(\text{Ba}_{1-x}\text{K}_x)\text{Fe}_2\text{As}_2$, *Phys. Rev. Lett.* **101**, 107006 (2008).
- [10] Z. Bukowski, S. Weyeneth, R. Puzniak, P. Moll, S. Katrych, N. D. Zhigadlo, J. Karpinski, H. Keller, and B. Batlogg, Superconductivity at 23 K and low anisotropy in Rb-substituted BaFe_2As_2 single crystals, *Phys. Rev. B* **79**, 104521 (2009).
- [11] M. G. Kim, A. Kreyssig, A. Thaler, D. K. Pratt, W. Tian, J. L. Zarestky, M. A. Green, S. L. Bud'ko, P. C. Canfield, R. J. McQueeney, and A. I. Goldman, Antiferromagnetic ordering in the absence of structural distortion in $\text{Ba}(\text{Fe}_{1-x}\text{Mn}_x)_2\text{As}_2$, *Phys. Rev. B* **82**, 220503(R) (2010).
- [12] A. Thaler, H. Hodovanets, M. S. Torikachvili, S. Ran, A. Kracher, W. Straszheim, J. Q. Yan, E. Mun, and P. C. Canfield,

- Physical and magnetic properties of $\text{Ba}(\text{Fe}_{1-x}\text{Mn}_x)_2\text{As}_2$ single crystals, *Phys. Rev. B* **84**, 144528 (2011).
- [13] A. Pandey, V. K. Anand, and D. C. Johnston, Large miscibility gap in the $\text{Ba}(\text{Mn}_x\text{Fe}_{1-x})_2\text{As}_2$ system, *Phys. Rev. B* **84**, 014405 (2011).
- [14] Y. Texier, Y. Laplace, P. Mendels, J. T. Park, G. Friemel, D. L. Sun, D. S. Inosov, C. T. Lin, and J. Bobroff, Mn local moments prevent superconductivity in iron pnictides $\text{Ba}(\text{Fe}_{1-x}\text{Mn}_x)_2\text{As}_2$, *EPL (Europhysics Letters)* **99**, 17002 (2012).
- [15] H. Suzuki, T. Yoshida, S. Ideta, G. Shibata, K. Ishigami, T. Kadono, A. Fujimori, M. Hashimoto, D. H. Lu, Z.-X. Shen, K. Ono, E. Sakai, H. Kumigashira, M. Matsuo, and T. Sasagawa, Absence of superconductivity in the hole-doped Fe pnictide $\text{Ba}(\text{Fe}_{1-x}\text{Mn}_x)_2\text{As}_2$: Photoemission and x-ray absorption spectroscopy studies, *Phys. Rev. B* **88**, 100501(R) (2013).
- [16] G. S. Tucker, D. K. Pratt, M. G. Kim, S. Ran, A. Thaler, G. E. Granroth, K. Marty, W. Tian, J. L. Zarestky, M. D. Lumsden, S. L. Bud'ko, P. C. Canfield, A. Kreyssig, A. I. Goldman, and R. J. McQueeney, Competition between stripe and checkerboard magnetic instabilities in Mn-doped BaFe_2As_2 , *Phys. Rev. B* **86**, 020503(R) (2012).
- [17] F. A. Garcia, O. Ivashko, D. E. McNally, L. Das, M. M. Piva, C. Adriano, P. G. Pagliuso, J. Chang, T. Schmitt, and C. Monney, Anisotropic magnetic excitations and incipient Néel order in $\text{Ba}(\text{Fe}_{1-x}\text{Mn}_x)_2\text{As}_2$, *Phys. Rev. B* **99**, 115118 (2019).
- [18] R. M. Fernandes and A. J. Millis, Suppression of superconductivity by Néel-type magnetic fluctuations in the iron pnictides, *Phys. Rev. Lett.* **110**, 117004 (2013).
- [19] M. N. Gastiasoro and B. M. Andersen, Enhancement of magnetic stripe order in iron-pnictide superconductors from the interaction between conduction electrons and magnetic impurities, *Phys. Rev. Lett.* **113**, 067002 (2014).
- [20] M. N. Gastiasoro, F. Bernardini, and B. M. Andersen, Unconventional disorder effects in correlated superconductors, *Phys. Rev. Lett.* **117**, 257002 (2016).
- [21] A. G. de Figueiredo, M. R. Cantarino, W. R. da Silva Neto, K. R. Pakuszewski, R. Grossi, D. S. Christovam, J. C. Souza, M. M. Piva, G. S. Freitas, P. G. Pagliuso, C. Adriano, and F. A. Garcia, Orbital localization and the role of the Fe and As $4p$ orbitals in BaFe_2As_2 probed by XANES, *Phys. Rev. B* **105**, 045130 (2022).
- [22] Y. X. Yao, J. Schmalian, C. Z. Wang, K. M. Ho, and G. Kotliar, Comparative study of the electronic and magnetic properties of BaFe_2As_2 and BaMn_2As_2 using the Gutzwiller approximation, *Phys. Rev. B* **84**, 245112 (2011).
- [23] A. Antal, T. Knoblauch, Y. Singh, P. Gegenwart, D. Wu, and M. Dressel, Optical properties of the iron-pnictide analog BaMn_2As_2 , *Phys. Rev. B* **86**, 014506 (2012).
- [24] D. E. McNally, S. Zellman, Z. P. Yin, K. W. Post, H. He, K. Hao, G. Kotliar, D. Basov, C. C. Homes, and M. C. Aronson, From Hund's insulator to Fermi liquid: Optical spectroscopy study of K doping in BaMn_2As_2 , *Phys. Rev. B* **92**, 115142 (2015).
- [25] T. M. Garitezi, C. Adriano, P. F. S. Rosa, E. M. Bittar, L. Bufaiçal, R. L. de Almeida, E. Granado, T. Grant, Z. Fisk, M. A. Avila, R. A. Ribeiro, P. L. Kuhns, A. P. Reyes, R. R. Urbano, and P. G. Pagliuso, Synthesis and characterization of BaFe_2As_2 single crystals grown by in-flux technique, *Braz. J. Phys.* **43**, 223 (2013).
- [26] D. S. Inosov, G. Friemel, J. T. Park, A. C. Walters, Y. Texier, Y. Laplace, J. Bobroff, V. Hinkov, D. L. Sun, Y. Liu, R. Khasanov, K. Sedlak, P. Bourges, Y. Sidis, A. Ivanov, C. T. Lin, T. Keller, and B. Keimer, Possible realization of an antiferromagnetic Griffiths phase in $\text{Ba}(\text{Fe}_{1-x}\text{Mn}_x)_2\text{As}_2$, *Phys. Rev. B* **87**, 224425 (2013).
- [27] P. Werner, E. Gull, M. Troyer, and A. J. Millis, Spin freezing transition and non-Fermi-liquid self-energy in a three-orbital model, *Phys. Rev. Lett.* **101**, 166405 (2008).
- [28] K. M. Stadler, G. Kotliar, S.-S. B. Lee, A. Weichselbaum, and J. von Delft, Differentiating Hund from Mott physics in a three-band Hubbard-Hund model: Temperature dependence of spectral, transport, and thermodynamic properties, *Phys. Rev. B* **104**, 115107 (2021).
- [29] See Supplemental Material at <http://link.aps.org/supplemental/10.1103/PhysRevB.108.245124>, for details of ARPES experiments and MDCs analysis.
- [30] M. Yi, Y. Zhang, Z.-X. Shen, and D. Lu, Role of the orbital degree of freedom in iron-based superconductors, *npj Quantum Mater.* **2**, 57 (2017).
- [31] V. Brouet, M. F. Jensen, P.-H. Lin, A. Taleb-Ibrahimi, P. Le Fèvre, F. Bertran, C.-H. Lin, W. Ku, A. Forget, and D. Colson, Impact of the two Fe unit cell on the electronic structure measured by ARPES in iron pnictides, *Phys. Rev. B* **86**, 075123 (2012).
- [32] M. Fuglsang Jensen, V. Brouet, E. Papalazarou, A. Nicolaou, A. Taleb-Ibrahimi, P. Le Fèvre, F. Bertran, A. Forget, and D. Colson, Angle-resolved photoemission study of the role of nesting and orbital orderings in the antiferromagnetic phase of BaFe_2As_2 , *Phys. Rev. B* **84**, 014509 (2011).
- [33] H. Pfau, C. R. Rotundu, J. C. Palmstrom, S. D. Chen, M. Hashimoto, D. Lu, A. F. Kemper, I. R. Fisher, and Z.-X. Shen, Detailed band structure of twinned and detwinned BaFe_2As_2 studied with angle-resolved photoemission spectroscopy, *Phys. Rev. B* **99**, 035118 (2019).
- [34] R. M. Fernandes, A. I. Coldea, H. Ding, I. R. Fisher, P. J. Hirschfeld, and G. Kotliar, Iron pnictides and chalcogenides: A new paradigm for superconductivity, *Nature (London)* **601**, 35 (2022).
- [35] Y. Zhang, F. Chen, C. He, B. Zhou, B. P. Xie, C. Fang, W. F. Tsai, X. H. Chen, H. Hayashi, J. Jiang, H. Iwasawa, K. Shimada, H. Namatame, M. Taniguchi, J. P. Hu, and D. L. Feng, Orbital characters of bands in the iron-based superconductor $\text{BaFe}_{1.85}\text{Co}_{0.15}\text{As}_2$, *Phys. Rev. B* **83**, 054510 (2011).
- [36] S. Thirupathiah, S. de Jong, R. Ovsyannikov, H. A. Dürr, A. Varykhalov, R. Follath, Y. Huang, R. Huisman, M. S. Golden, Y.-Z. Zhang, H. O. Jeschke, R. Valentí, A. Erb, A. Gloskovskii, and J. Fink, Orbital character variation of the Fermi surface and doping dependent changes of the dimensionality in $\text{BaFe}_{2-x}\text{Co}_x\text{As}_2$ from angle-resolved photoemission spectroscopy, *Phys. Rev. B* **81**, 104512 (2010).
- [37] R. M. Fernandes and A. V. Chubukov, Low-energy microscopic models for iron-based superconductors: A review, *Rep. Prog. Phys.* **80**, 014503 (2017).
- [38] V. Brouet, M. Marsi, B. Mansart, A. Nicolaou, A. Taleb-Ibrahimi, P. Le Fèvre, F. Bertran, F. Rullier-Albenque, A. Forget, and D. Colson, Nesting between hole and electron pockets in $\text{Ba}(\text{Fe}_{1-x}\text{Co}_x)_2\text{As}_2$ ($x = 0 - 0.3$) observed with angle-resolved photoemission, *Phys. Rev. B* **80**, 165115 (2009).
- [39] J. A. Sobota, Y. He, and Z.-X. Shen, Angle-resolved photoemission studies of quantum materials, *Rev. Mod. Phys.* **93**, 025006 (2021).

- [40] R. Kurlito and J. Fink, About two-dimensional fits for the analysis of the scattering rates and renormalization functions from angle-resolved photoelectron spectroscopy data, *J. Electron Spectrosc. Relat. Phenom.* **253**, 147127 (2021).
- [41] J. Fink, E. D. L. Rienks, M. Yao, R. Kurlito, J. Bannies, S. Aswartham, I. Morozov, S. Wurmehl, T. Wolf, F. Hardy, C. Meingast, H. S. Jeevan, J. Maiwald, P. Gegenwart, C. Felser, and B. Büchner, Linkage between scattering rates and superconductivity in doped ferropnictides, *Phys. Rev. B* **103**, 155119 (2021).
- [42] T. Shibauchi, A. Carrington, and Y. Matsuda, A quantum critical point lying beneath the superconducting dome in iron pnictides, *Annu. Rev. Condens. Matter Phys.* **5**, 113 (2014).
- [43] M. Merz, P. Schweiss, P. Nagel, M.-J. Huang, R. Eder, T. Wolf, H. von Loehneysen, and S. Schuppler, Of substitution and doping: Spatial and electronic structure in Fe pnictides, *J. Phys. Soc. Jpn.* **85**, 044707 (2016).
- [44] M. Yi, Y. Zhang, Z.-K. Liu, X. Ding, J.-H. Chu, A. F. Kemper, N. Plonka, B. Moritz, M. Hashimoto, S.-K. Mo, Z. Hussain, T. P. Devereaux, I. R. Fisher, H. H. Wen, Z.-X. Shen, and D. H. Lu, Dynamic competition between spin-density wave order and superconductivity in underdoped $\text{Ba}_{1-x}\text{K}_x\text{Fe}_2\text{As}_2$, *Nat. Commun.* **5**, 3711 (2014).
- [45] M. Yi, Z.-K. Liu, Y. Zhang, R. Yu, J.-X. Zhu, J. J. Lee, R. G. Moore, F. T. Schmitt, W. Li, S. C. Riggs, J.-H. Chu, B. Lv, J. Hu, M. Hashimoto, S.-K. Mo, Z. Hussain, Z. Q. Mao, C. W. Chu, I. R. Fisher, Q. Si *et al.*, Observation of universal strong orbital-dependent correlation effects in iron chalcogenides, *Nat. Commun.* **6**, 7777 (2015).
- [46] J. Zaanen, Why the temperature is high, *Nature (London)* **430**, 512 (2004).
- [47] P. Richard, A. van Roekeghem, B. Q. Lv, T. Qian, T. K. Kim, M. Hoesch, J.-P. Hu, A. S. Sefat, S. Biermann, and H. Ding, Is BaCr_2As_2 symmetrical to BaFe_2As_2 with respect to half 3d shell filling?, *Phys. Rev. B* **95**, 184516 (2017).
- [48] H. Wadati, I. Elfimov, and G. A. Sawatzky, Where are the extra d electrons in transition-metal-substituted iron pnictides?, *Phys. Rev. Lett.* **105**, 157004 (2010).
- [49] T. Valla, A. V. Fedorov, P. D. Johnson, and S. L. Hulbert, Many-body effects in angle-resolved photoemission: Quasiparticle energy and lifetime of a Mo (110) surface state, *Phys. Rev. Lett.* **83**, 2085 (1999).
- [50] J. Nayak, K. Filsinger, G. H. Fecher, S. Chadov, J. Minar, E. D. L. Rienks, B. Büchner, S. P. Parkin, J. Fink, and C. Felser, Observation of a remarkable reduction of correlation effects in BaCr_2As_2 by ARPES, *Proc. Natl. Acad. Sci. USA* **114**, 12425 (2017).
- [51] Z. R. Ye, Y. Zhang, F. Chen, M. Xu, J. Jiang, X. H. Niu, C. H. P. Wen, L. Y. Xing, X. C. Wang, C. Q. Jin, B. P. Xie, and D. L. Feng, Extraordinary doping effects on quasiparticle scattering and bandwidth in iron-based superconductors, *Phys. Rev. X* **4**, 031041 (2014).
- [52] T. Kawashima, S. Miyasaka, H. Tsuji, T. Yamamoto, M. Uekubo, A. Takemori, K. T. Lai, and S. Tajima, Importance of d_{xy} orbital and electron correlation in iron-based superconductors revealed by phase diagram for 1111-system, *Sci. Rep.* **11**, 10006 (2021).
- [53] C. M. Varma, *Colloquium: Linear in temperature resistivity and associated mysteries including high temperature superconductivity*, *Rev. Mod. Phys.* **92**, 031001 (2020).
- [54] J. Fink, E. D. L. Rienks, S. Thirupathiah, J. Nayak, A. van Roekeghem, S. Biermann, T. Wolf, P. Adelman, H. S. Jeevan, P. Gegenwart, S. Wurmehl, C. Felser, and B. Büchner, Experimental evidence for importance of Hund's exchange interaction for incoherence of charge carriers in iron-based superconductors, *Phys. Rev. B* **95**, 144513 (2017).
- [55] P. Werner, M. Casula, T. Miyake, F. Aryasetiawan, A. J. Millis, and S. Biermann, Satellites and large doping and temperature dependence of electronic properties in hole-doped BaFe_2As_2 , *Nat. Phys.* **8**, 331 (2012).
- [56] E. Bascones, B. Valenzuela, and M. Jose Calderon, Magnetic interactions in iron superconductors: A review, *C. R. Phys.* **17**, 36 (2016).
- [57] L. Fanfarillo and E. Bascones, Electronic correlations in Hund metals, *Phys. Rev. B* **92**, 075136 (2015).
- [58] L. de' Medici, G. Giovannetti, and M. Capone, Selective Mott physics as a key to iron superconductors, *Phys. Rev. Lett.* **112**, 177001 (2014).
- [59] T. Berlijn, C.-H. Lin, W. Garber, and W. Ku, Do transition-metal substitutions dope carriers in iron-based superconductors?, *Phys. Rev. Lett.* **108**, 207003 (2012).
- [60] T. Kobayashi, M. Nakajima, S. Miyasaka, and S. Tajima, Carrier localization due to local magnetic order induced by magnetic impurities in $\text{Ba}(\text{Fe}_{1-x}\text{TM}_x)_2\text{As}_2$ ($\text{TM} = \text{Mn}$ and Cr) as seen via optical spectra, *Phys. Rev. B* **94**, 224516 (2016).
- [61] G. Levy, R. Sutarto, D. Chevrier, T. Regier, R. Blyth, J. Geck, S. Wurmehl, L. Harnagea, H. Wadati, T. Mizokawa, I. S. Elfimov, A. Damascelli, and G. A. Sawatzky, Probing the role of Co substitution in the electronic structure of iron pnictides, *Phys. Rev. Lett.* **109**, 077001 (2012).
- [62] S. Ideta, T. Yoshida, I. Nishi, A. Fujimori, Y. Kotani, K. Ono, Y. Nakashima, S. Yamaichi, T. Sasagawa, M. Nakajima, K. Kihou, Y. Tomioka, C. H. Lee, A. Iyo, H. Eisaki, T. Ito, S. Uchida, and R. Arita, Dependence of carrier doping on the impurity potential in transition-metal-substituted FeAs-based superconductors, *Phys. Rev. Lett.* **110**, 107007 (2013).
- [63] M. D. Watson, P. Dudin, L. C. Rhodes, D. V. Evtushinsky, H. Iwasawa, S. Aswartham, S. Wurmehl, B. Büchner, M. Hoesch, and T. K. Kim, Probing the reconstructed Fermi surface of antiferromagnetic BaFe_2As_2 in one domain, *npj Quantum Mater.* **4**, 36 (2019).
- [64] A. Fedorov, A. Yaresko, E. Haubold, Y. Kushnirenko, T. Kim, B. Büchner, S. Aswartham, S. Wurmehl, and S. Borisenko, Energy scale of nematic ordering in the parent iron-based superconductor BaFe_2As_2 , *Phys. Rev. B* **100**, 024517 (2019).
- [65] Y. Zhang, M. Yi, Z.-K. Liu, W. Li, J. J. Lee, R. G. Moore, M. Hashimoto, M. Nakajima, H. Eisaki, S.-K. Mo, Z. Hussain, T. P. Devereaux, Z.-X. Shen, and D. H. Lu, Distinctive orbital anisotropy observed in the nematic state of a FeSe thin film, *Phys. Rev. B* **94**, 115153 (2016).
- [66] M. Yi, D. Lu, J.-H. Chu, J. G. Analytis, A. P. Sorini, A. F. Kemper, B. Moritz, S.-K. Mo, R. G. Moore, M. Hashimoto, W.-S. Lee, Z. Hussain, T. P. Devereaux, I. R. Fisher, and Z.-X. Shen, Symmetry-breaking orbital anisotropy observed for

- detwinned $\text{Ba}(\text{Fe}_{1-x}\text{Co}_x)_2\text{As}_2$ above the spin density wave transition, *Proc. Natl. Acad. Sci. USA* **108**, 6878 (2011).
- [67] X. Wang and R. M. Fernandes, Impact of local-moment fluctuations on the magnetic degeneracy of iron arsenide superconductors, *Phys. Rev. B* **89**, 144502 (2014).
- [68] J. Pelliciari, K. Ishii, Y. Huang, M. Dantz, X. Lu, P. Olalde-Velasco, V. N. Strocov, S. Kasahara, L. Xing, X. Wang, C. Jin, Y. Matsuda, T. Shibauchi, T. Das, and T. Schmitt, Reciprocity between local moments and collective magnetic excitations in the phase diagram of $\text{BaFe}_2(\text{As}_{1-x}\text{Px})_2$, *Commun. Phys.* **2**, 139 (2019).
- [69] J. Pelliciari, K. Ishii, M. Dantz, X. Lu, D. E. McNally, V. N. Strocov, L. Xing, X. Wang, C. Jin, H. S. Jeevan, P. Gegenwart, and T. Schmitt, Local and collective magnetism of EuFe_2As_2 , *Phys. Rev. B* **95**, 115152 (2017).
- [70] K.-J. Zhou, Y.-B. Huang, C. Monney, X. Dai, V. N. Strocov, N.-L. Wang, Z.-G. Chen, C. Zhang, P. Dai, L. Patthey, J. van den Brink, H. Ding, and T. Schmitt, Persistent high-energy spin excitations in iron-pnictide superconductors, *Nat. Commun.* **4**, 1470 (2013).
- [71] E. Kaneshita, K. Tsutsui, and T. Tohyama, Spin and orbital characters of excitations in iron arsenide superconductors revealed by simulated resonant inelastic x-ray scattering, *Phys. Rev. B* **84**, 020511(R) (2011).
- [72] M. Xu, J. Schmidt, E. Gati, L. Xiang, W. R. Meier, V. G. Kogan, S. L. Bud'ko, and P. C. Canfield, Superconductivity and phase diagrams of $\text{CaK}(\text{Fe}_{1-x}\text{Mn}_x)_4\text{As}_4$ single crystals, *Phys. Rev. B* **105**, 214526 (2022).
- [73] M. Xu, J. Schmidt, M. A. Tanatar, R. Prozorov, S. L. Bud'ko, and P. C. Canfield, Superconductivity and magnetic and transport properties of single-crystalline $\text{CaK}(\text{Fe}_{1-x}\text{Cr}_x)_4\text{As}_4$, *Phys. Rev. B* **107**, 134511 (2023).
- [74] L. Chen, C. Cao, H. Chen, J. Guo, J. Ma, J. Hu, and G. Wang, Miscibility gap and possible intrinsic Griffiths phase in $\text{Sr}(\text{Fe}_{1-x}\text{Mn}_x)_2\text{As}_2$ crystals grown by transition metal arsenide flux, *Phys. Rev. B* **103**, 134509 (2021).
- [75] N. Giovanni, M. Civelli, and M. C. O. Aguiar, Anderson localization effects on the doped Hubbard model, *Phys. Rev. B* **103**, 245134 (2021).
- [76] E. C. Andrade, E. Miranda, and V. Dobrosavljević, Electronic Griffiths phase of the $d = 2$ Mott transition, *Phys. Rev. Lett.* **102**, 206403 (2009).
- [77] D. Tanasković, E. Miranda, and V. Dobrosavljević, Effective model of the electronic Griffiths phase, *Phys. Rev. B* **70**, 205108 (2004).